Journal of
Materials Chemistry C

Materials for optical, magnetic and electronic devices

Accepted Manuscript

Journal of
Materials Chemistry C

Materials for optical, magnetic and electronic devices

rsc.li/materials-c

Volume 6
Number 5
7 February 2018
Pages 911-1266

ISSN 2050-7526

ROYAL SOCIETY OF CHEMISTRY

PAPER
Nosang V. Myung, Yong-Ho Choe et al.
A noble gas sensor platform: linear dense assemblies of single-walled carbon nanotubes (LACNTs) in a multi-layered ceramic/metal electrode system (MLES)

This is an Accepted Manuscript, which has been through the Royal Society of Chemistry peer review process and has been accepted for publication.

Accepted Manuscripts are published online shortly after acceptance, before technical editing, formatting and proof reading. Using this free service, authors can make their results available to the community, in citable form, before we publish the edited article. We will replace this Accepted Manuscript with the edited and formatted Advance Article as soon as it is available.

You can find more information about Accepted Manuscripts in the Information for Authors.

ROYAL SOCIETY OF CHEMISTRY

rsc.li/materials-c

ARTICLE

Revealing Internal Heavy Chalcogen Atom Effect on the Photophysics of Dibenzo[*a,j*]phenazine-Cored Donor–Acceptor–Donor Triad

Shimpei Goto,[a] Yuya Nitta,[a] Nicolas Oliveira Decarli,[b] Leonardo Evaristo de Sousa,[c] Patrycja Stachelek,[d] Norimitsu Tohnai,[a] Satoshi Minakata,[a] Piotr de Silva,*[c] Przemyslaw Data*[be], and Youhei Takeda*[a]

A new twisted donor–acceptor–donor (D–A–D) multi-photofunctional organic molecule comprising of phenoselenazine as the electron-donors (Ds) and dibenzo[*a,j*]phenazine (DBPHZ) as the electron-acceptor (A) has been developed. The developed selenium-incorporated D–A–D compound is featured with multi-color polymorphism, distinct mechanochromic luminescence, chemically-stimulated luminochromism, thermally-activated delayed fluorescence, and room-temperature phosphorescence. The internal heavy atom effect on the photophysical properties of the D–A–D system has been investigated through the comparison with the physicochemical properties of a previously developed sulfur analogue and a tellurium analogue.

INTRODUCTION

Selenium (Se) and Tellurium (Te), that are heavier congeners of Sulfur (S), have a very similar and lower electronegativity (χ_P) with Sulfur (Se: 2.55, Te: 2.10, S: 2.58), respectively, and they have slight larger covalent radius than that of sulfur (Se: 1.17 Å, Te: 1.38 Å, S: 1.04 Å). Owing to such electronic and structural perturbation, the replacement of the S atoms of an organosulfur compound with Se or Te atoms leads to a drastic change in reactivity and physicochemical property. Such "internal heavy atom effect" have fascinated scientists, and indeed a myriad of functional organo-selenium and -tellurium compounds have been developed. Nowadays, they can find diverse applications in a range of fields such as biology,[1] medicinal chemistry,[1,2] chemical biology,[3] synthetic chemistry,[4] catalysis sciences,[5] polymer sciences,[6] and materials sciences.[7] In this context, planar π-conjugated molecules and polymers decorated with Se and/or Te at the main π-conjugated frameworks or at the peripherals of the π-systems have attracted considerable attention as functional materials for organic electronics. In addition to the intrinsic planar and rigid π-systems, the presence of Se/Te atoms results in not only strong intermolecular π-orbital interactions but also electrostatic interactions (i.e., chalcogen-bonding) in the solid states,[8] allowing for efficient charge carrier transport. Thus, some classes of compounds, such as seleno-/telluroarenes, seleno-/tellurophenes, and their oligomeric and polymeric derivatives, have emerged as promising organic semiconducting materials, and they find applications in organic field-effect transistors (OFETs),[9] organic photovoltaics (OPVs),[10] and organic thermoelectronics (OTEs).[11]

In stark contrast, organoselenium and organotellurium compounds displaying luminescence in the solid states have been less developed, and thereby the optoelectronic applications thereof are in their infancy.[12] The incorporation of selenium and other heavy atoms such as halogens into a luminogenic scaffold often generates the pair of singlet excited state $^1(n,\pi^*)$ (S_1) and triplet excited state $^3(\pi,\pi^*)$ (T_1) or $^1(\pi,\pi^*)$ and $^3(n,\pi^*)$. In conjunction with the intrinsically large spin-orbit coupling (SOC) constant (ζ_{SO}) of Se (ca. 5.07 kcal/mol) and Te (ca. 11.3 kcal/mol),[13] the SOC matrix element (H_{SOC}) for the S_1–T_1 transition of a Se- or Te-containing π-conjugated compound becomes large, allowing the spin-forbidden S–T transitions.[14] Therefore, upon photo-excitation, the T_1 state of an organoselenium/tellurium molecule is promptly populated through a rapid intersystem crossing (ISC) from the S_1 state.[15] With a well-studied planar π-conjugated

a. Department of Applied Chemistry, Graduate School of Engineering, Osaka University, Yamadaoka 2-1, Suita, Osaka 565-0871, Japan.
   E-mail: takeda@chem.eng.osaka-u.ac.jp
b. Faculty of Chemistry, Silesian University of Technology, M. Strzody 9, 44-100 Gliwice, Poland.
   E-mail: przemyslaw.data@polsl.pl
c. Department of Energy Conversion and Storage, Technical University of Denmark, Anker Engelunds Vej 301, 2800 Kongens Lyngby, Denmark.
   E-mail: pdes@dtu.dk
d. Durham University, Chemistry Department, South Road, Durham DH1 3LE, United Kingdom.
e. Centre of Polymer and Carbon Materials, Polish Academy of Science, M. Curie-Sklodowskiej 34, 41-819, Zabrze, Poland.

ARTICLE

organoselenium/tellurium frameworks, the singlet-triplet energy splitting (ΔE_{ST}) is relatively large comparable with other acene analogues, and as mentioned-above, the intermolecular interactions are strong in the solid states. As the results of intrinsic large SOC induced by Se and Te, ISC from the S_1 to T_1 is allowed, and thereby T_1 state in the solids would be just depopulated through non-irradiative pathways such as thermal internal conversion (IC) via bond rotations and molecular vibrations, and energy diffusion.

Over the last few years, the internal heavy atom effects on the optoelectronic properties of triplet-harvesting organoselenium emitters based on twisted D–π–A[16,17] and D–π–D[18] scaffolds displaying thermally activated delayed fluorescence (TADF)[19] and room-temperature phosphorescence (RTP)[20] have been reported (Fig. 1). In 2019, de Sa Pereira, Kukhta, and Lee investigated the effect of replacing Se for S atom of a D–π–A TADF emitter on the photophysics through a sophisticated time-resolved spectroscopic analysis of D_{Se}–π–A type compound **PSeZ-TRZ** (Fig. 1a) in comparison with that of its sulfur TADF emitter **PTZ-TRZ**.[16] The analysis of the complicated decays of **PSeZ-TRZ** in non-polar polymer matrix Zeonex® rationally explained the independent radiative pathways of two conformers, i.e., quasi-axial (ax) and quasi-equatorial (eq) (Fig. 1a). Most importantly, replacing Se for S does not affect the reverse ISC (rISC) in significant degree but so does room-temperature phosphorescence (RTP) efficiency of the donor. On the other hand, Credgington and Seferos investigated the effect of

replacing Se for S of a TADF compound **TXO₁-TPA** on ISC and rISC processes by developing a D–π–A$_{Se}$ type compound **SeXO₁-TPA** (Fig. 1b).[17] The detailed kinetic analysis revealed that the Se affects both of ISC and rISC rates, enhancing the ISC more than 250 times and the rISC 22 time faster than those of the sulfur TADF emitter. Given these apparently contradicting results, the position of Se atom on π-electron systems significantly affect the photophysical properties of the selenium-embedded compounds. Most recently, Kim and Lee developed D_{Se}–π–D_{se} type metal-free RTP compounds **PSe1**, **PSe2**, and **PSe3** (Fig. 1c) for OLEDs. The authors claimed that the n-π* transitions involving differentially-oriented p orbitals on the Se atom ($p_z \rightarrow p_{xy}$) significantly enhance the H_{SOC} between the S_0 and T_1, thereby accelerating the radiation from the T_1 state.[18] Zhao and Huang reported the effect of chalcogen atoms in the chalcogenophene–π-phenylcarbazoles on the optoelectronic properties and revealed dual emission behavior of fluorescence and RTP.[21] He and co-workers developed a D–A$_{Se}$–D type organic phosphorescent compound for afterglow imaging and photodynamic therapy by taking the advantage of long-lived triplet excited states.[22] Therefore, investigation on the effect of replacing Se/Te for S atoms of TADF/RTP-active compounds on their photophysical properties would provide profound insights into understanding the design principles for balancing conflicting factors ΔE_{ST} and SOC to realize novel chalcogen-containing organic photofunctional materials.

Herein we disclose the development of novel twisted donor-acceptor-donor (D–A–D) organic emitters **PSeZ-DBPHZ-PSeZ** and **PTeZ-DBPHZ-PTeZ** based on a new organoselnium/tellurium scaffold (D_{Se}–A–D_{Se} and D_{Te}–A–D_{Te}, respectively) (Fig. 1d). Most importantly, the investigation of their physicochemical properties revealed that **PSeZ-DBPHZ-PSeZ** is multi-photofunctional material featured with polymorphs-dependent multi emission colors, single-molecular white emission (SMWE), mechanochromic luminescence (MCL), chemical stimuli-responsive emission change, and distinct delayed emission in matrices and organic light-emitting diodes (OLEDs) (Fig. 1d). The comparison of the experimental properties and quantum chemical calculation data of the series of D–A–D compounds clarified that the conformational preference arising from the "ax" and "eq" donors is strongly correlated with the chalcogen atoms and thus governs their photophysical properties.

Fig. 1 a)–c) Structures of previously reported TADF- and RTP-active organoselenium compounds; d) Structures of newly developed D–A–D type organoselenium and tellurium compounds.

RESULTS AND DISCUSSION

Design and Synthesis

Previously, we have developed multi-photofunctional organic materials displaying thermally activated delayed fluorescence (TADF), mechanochromic luminescence (MCL),[23] and room-temperature phosphorescence (RTP) properties, based on a donor–acceptor–donor (D–A–D)[24–29] or a D–A–D–A scaffold,[30] utilizing dibenzo[*a,j*]phenazine (DBPHZ)[31] as the key acceptor unit. In 2017, we reported the first example of TADF-active multi-color-changing MCL material (**PTZ-DBPHZ-PTZ**) based on
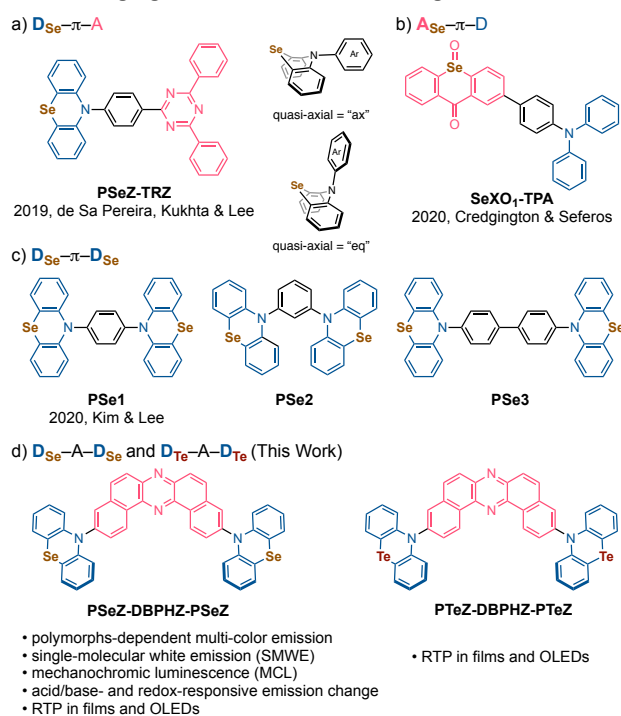
the design concept of conformation-dictated regulation of luminescence properties, where the ax- and eq-conformer arising from the boat-chair geometry of phenothiazine plays the key role in giving divergent ground and excited state energies.[26a] To reveal the effect of replacing Se/Te for S of **PTZ-DBPHZ-PTZ**, D–A–D compounds on the photo-functionality, **PSeZ-DBPHZ-PSeZ** and **PTeZ-DBPHZ-PTeZ** were designed (Fig. 1d). **PSeZ-DBPHZ-PSeZ** was successfully synthesized through a Pd-catalyzed Buchwald-Hartwig double amination of 3,11-dibromo-dibenzo[*a,j*]phenazine (**Br2-DBPHZ**)[31] with phenoselenazine (**PSeZ**) in a good yield (the upper equation in Scheme 1). The product was further purified through recrystallization from CH_2Cl_2/*n*-Hex solution to give yellow powdery solids. The product was fully characterized by ^{1}H, ^{13}C, & ^{77}Se NMR, X-ray crystallography, mass spectroscopy, IR spectroscopy, and elemental analysis (for the details, see the Synthetic Procedures and Spectroscopic Data in the ESI). **PTeZ-DBPHZ-PTeZ** was also synthesized through an amination of **Br2-DBPHZ** with phoenotellurazine (**PTeZ**) (the bottom equation in Scheme 1; see the Synthetic Procedures and Spectroscopic Data in the ESI). In stark contrast to **PSeZ**, the known synthetic method for **PTeZ** is far from practical, due to the use of toxic mercury reagent.[32] Therefore, we decided to establish an up-dated synthetic method for **PTeZ** by modifying our method for phosphorous-bridged diarylamine (dihydrophenophosphanizine).[27] As the results, the cyclization of dilithiated *N*-Boc diarylamine with $TeCl_4$ followed by the reduction of the resulting Te(IV) center successfully gave **PTeZ** (for the detail procedures, see the ESI). Incidentally, during the preparation of this manuscript, the Patureau group also reported a robust synthetic method for **PTeZ** using Te(0) as the tellurium source.[33] It is noted that **PTeZ-DBPHZ-PTeZ** represents the first example of D–A type emissive compounds that have phenotellurazine (**PTeZ**) as the electron donor.
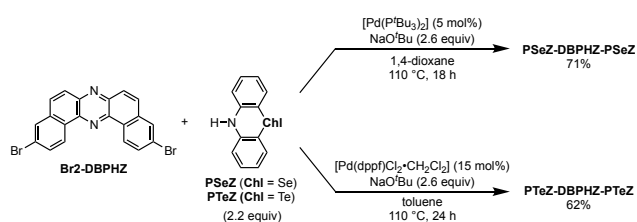
Scheme 1 Synthesis of **PSeZ-DBPHZ-PSeZ** and **PTeZ-DBPHZ-PTeZ**.

Polymorphisms

Through our attempts to recrystallize **PSeZ-DBPHZ-PSeZ** from various solvent systems, we serendipitously found out that the molecule forms 3 different concomitant polymorphs (denoted as **G**, **Y**, and **O**; for the detailed X-ray crystallographic data, see the Table S1–S3 and Fig. S1–S3) grown from the same *n*-Hex/EtOAc solution. Notably, those polymorphs displayed distinctly different photoluminescence colors (green, yellow, and orange) under the irradiation of a UV light (Fig. 2a). As the results of screening of solvent systems for selective

preparation of those polymorphs, we found out that the recrystallization from a $CHCl_3$/*n*-Hex solution exclusively gave polymorph **Y**, while CH_2Cl_2/AcOEt solvent system provided polymorph **O**. The characterization of these polymorphs obtained from different solvent systems were confirmed by the identification of experimental and simulated powder X-ray diffraction (PXRD) patterns. Unfortunately, we were not able to find solvent system to exclusively provide polymorph **G** after extensive attempts. The PL spectra of polymorphs **Y** and **O** clearly show significant difference in emission profiles ([Y]λ_{em} 546 nm, [Y]Φ_{PL} 0.02; [O]λ_{em} 666 nm, [O]Φ_{PL} 0.03) (Fig. 2b). Due to the scarcity of the amounts of the **G** polymorphs, the PL spectra were not collected. To investigate the origin of the significant difference in emission colors of those polymorphs, the X-ray crystallographic analyses were conducted (Fig. 2c–k). Unexpectedly, the emission difference stems from not only the different conformational geometries (i.e, **G**: ax-ax conformer; **Y** and **O**: eq-ax conformers, Fig. 2c–e) but also the different packing modes (Fig. 2f–k). In all the polymorphs, anti-parallel dimeric pairs were found with close interplane distance (d_{inter}) between the two adjacent DBZPH units (d_{inter} 3.27–3.47 Å), which cancel out dipole moments (Fig. 2i–k, Fig. S1–S3). Close look at the packing structures of **Y** and **O** revealed the distinct difference in d_{inter} and the degree of overlap of the π unit of the acceptor (DBPHZ) (Fig. 2j and k). From the comparison with the packing structure of previously reported sulfur-analogue **PTZ-DBPHZ-PTZ** in orange emitting single crystal (eq-ax
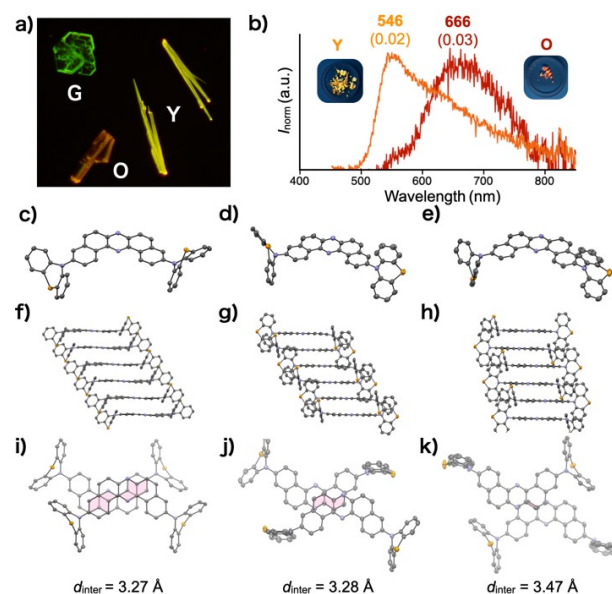

Fig. 2 a) A photograph of concomitant polymorphs **G**, **Y**, and **O** under the irradiation of a UV lamp (λ = 365 nm); b) PL spectra of **Y** and **O** (λ_{ex} = 340 nm; values in parentheses indicate the PLQY determined with an integral sphere); molecular structures of **PSeZ-DBPHZ-PSeZ** in c) **G**, d) **Y**, and e) **O**; packing structures of **PSeZ-DBPHZ-PSeZ** in f) **G**, g) **Y**, and h) **O**; dimeric pairs of **PSeZ-DBPHZ-PSeZ** with the closest d_{inter} value in i) **G**, j) **Y**, and k) **O** polymorphs. The pale pink region indicates the overlap area of π-moieties.

ARTICLE

conformation, λ_{em} 640 nm),[26a] it turned out that the packing structure of the selenium D–A–D compound in polymorph **O** is very similar to that of **PTZ-DBPHZ-PTZ** in the orange-emitting crystal, where the overlap of the π-unit in the dimeric pair and d_{inter} (3.46 Å) is almost the same. Taken together, we can conclude that the difference in emission profiles among the polymorphs of **PSeZ-DBPHZ-PSeZ** are not only determined by the molecular conformations but also the intermolecular electronic interactions.[34]

In contrast to the selenium D–A–D compound, any single crystals of tellurium containing compound **PTeZ-DBPHZ-PTeZ** suitable for X-ray crystallographic analysis were not obtained even after many attempts, due to powdery nature of the compound.

Steady-State Photophysical Properties in Solutions

To clarify the single molecular photophysical properties of the D–A–D compounds, the steady-state UV-vis absorption and photoluminescence spectra of dilute solutions (*c* = 10^{-5} M) in various solvents were acquired (Fig. 3, Table 1, Fig. S4, and Table S4). The Se-containing compound **PSeZ-DBPHZ-PSeZ** in dichloromethane displays a quite different absorption spectrum from the superposition of the individual spectra of D (**PSeZ**) and A (**DBPHZ**) (2D +A, Fig. 3a). The disappearance of the vibronic absorptions (ca. λ 300 nm and 380–420 nm) derived from the acceptor unit indicates a strong electronic coupling between the D and A units (Fig. 3a). This implies a quite different conformation of the Se compound from its sulfur analogue, where eq-eq conformer dominates and efficiently electron-decoupled absorption spectra displays.[26a] In a similar manner with our previously developed DBPHZ-cored D–A–D compounds,[25–29] an intramolecular charge-transfer (ICT) transition at around λ 460 nm was observed (Fig. 3a). However, when compared to the absorption spectra of the sulfur analogue, the molar coefficient (ca. ε 25,000–28,000) of the ICT band of the selenium compound is much larger than that of sulfur compound (ca. ε 10,000).[26a]

A similar trend in the absorption spectra was observed for tellurium-containing compound **PTeZ-DBPHZ-PTeZ**, where more distinct vibronic structure in the lowest-energy absorption regime ranging from 420 to 480 nm was dominated than the selenium compound (Fig. S4 and Table S4). This distinct difference caused by the Se and Te replacement for S atom suggests the ax-ax conformer is more dominated than sulfur analogue in solutions, which was supported by the theoretical calculations (*vide infra*). The comparison of the conformational population of the D–A–D compounds with each chalcogen-bridged diarylamine donor (S, Se, and Te) calculated by a Boltzmann weighted average of each conformer's equilibrium structure energy is illustrated in Fig. 3b. The effect of Se replacement for S in the D–A–D scaffold includes the switching of the majority conformer from eq-eq (ca. 59% contribution for the sulfur compound) to ax-ax (ca. 55% contribution for the selenium compound; ca. 98% contribution for the tellurium compound; Table S5–7). Importantly, energy decomposition analysis (EDA)[35] shows that

the conformational preference results from an interplay between Pauli, electrostatic, and orbital relaxation factors (Table S9). All these terms are strongly coupled to the equilibrium geometry. Nevertheless, substituting S with Se and Te in the D–A–D scaffold at a fixed geometry always leads to the relative stabilization of the axial conformer by Pauli repulsion and its destabilization by electrostatic and orbital relaxation. Given that the destabilizing Pauli energy accounts
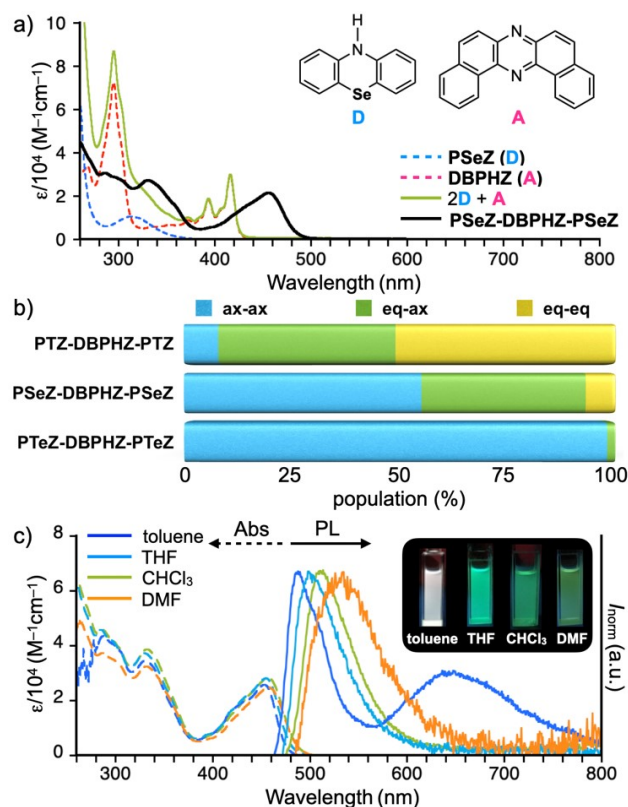

Fig. 3 a) Steady-state UV-vis absorptions of DCM solutions (*c* = 10^{-5} M) of **PSeZ** (cyan dotted line), **DBPHZ** (pink dotted line), 2D+A (moth solid line), and **PSeZ-DBPHZ-PSeZ** (black solid line); b) Conformational population of D–A–D compounds with S, Se, and Te donors in vacuum at 300 K calculated based on a Boltzmann weighted average of each conformer's equilibrium structure energy; c) Steady-state UV-vis absorption and photoluminescence (PL) spectra of solutions (*c* = 10^{-5} M, λ_{ex} = 400 nm) of **PSeZ-DBPHZ-PSeZ** prepared from various solvents. The inset photographs indicate the solutions taken under the irradiation of a UV light (λ = 365 nm).

Table 1 Summary of steady-state photophysical properties of **PSeZ-DBPHZ-PSeZ** in solutions (c = 10^{-5} M).

solvent	λ_{abs} (nm)	ε (M^{-1}cm^{-1})	λ_{em} (nm)	$\Phi_{PL}{}^a$
Toluene	453	25,800	480, 644	0.04
THF	454	28,200	493	0.01
CHCl$_3$	456	28,400	504	0.02
DMF	457	24,900	520	0.01

^{a}Determined with an integrating sphere.

for electronic repulsion, the thermodynamic preference of ax-ax conformers over eq-eq conformers in the selenium and tellurium-containing D–A–D compounds would be rationalized by less transannular electronic repulsion between the lone pairs on the N and the chalcogen atoms in the boat-chair donor unit.

The absorption spectra of **PSeZ-DBPHZ-PSeZ** were not affected by solvent polarity, suggesting the almost constant distribution of the conformers (dotted lines, Fig. 3c). The weak effect of solvent polarity on the conformer distribution is also confirmed by theoretical calculations as shown in Table S7. The difference in the absorption spectra between S, Se, and Te-containing D–A–D compounds is also fully explained by different conformer stability. The theoretical spectra calculated by weighting contributions from all the conformers agree with the experiments in terms of both relative band positions and their intensities (Table S10, S11, and Fig. S5).

Not only the absorption, the impact of the Se replacement was drastic in photoluminescence (PL) spectra as well. Most importantly, the toluene solution of **PSeZ-DBPHZ-PSeZ** displayed a dual emission peaked at λ 480 nm and 644 nm, thereby giving white emission (the photograph in Fig. 3c). This is a remarkable contrast with the sulfur compound: it only gives a broad Gaussian-type CT emission at around λ 657 nm in toluene.[26a] This should be associated with the dominance of the orthogonally-structured conformers (eq-eq and eq-ax) in the sulfur compound, which generates distinctly charge-separated CT excited states and relaxed in a polar solvent. The Se replacement affects the thermodynamic stability of the conformers, and thereby the admixture of the greenish LE emission at around λ 480 nm from the dominant ax-ax conformer and the CT emissions from eq-ax (~38%) and eq-eq (~8%) conformers should yield white emission. Recently, single molecular white emitters (SMWEs) have emerged as promising materials for optoelectronic and sensor applications.[36] Nevertheless, the rational design of SMWEs is difficult, due to the energy transfer problems, for instance. Therefore, the introduction of **PSeZ** donors in D–A–D scaffold allows for strategic design of SMWEs by mixing ax-ax and eq-based conformers to balance energetically-different emissions. As the polarity of solvent increases, the LE emission at around 480 nm in toluene gradually red-shifted, while the CT emission at around 650 nm in toluene was totally vanished (Fig. 3c). This polarity-dependence would support the significant difference in CT natures of the two emissions observed in toluene: the bluer emission is LE with a weak CT nature yielded from ax-ax conformer, while redder emission is derived from a stabilized CT excited state with a highly twisted structure (twisted intramolecular charge-transfer: TICT state) from eq-ax and eq-eq conformers. Due to the distinct charge separation, the redder emission is highly susceptible to solvent polarity, and in more polar solvent than toluene, the lower CT excited state is dissipated through atomic vibrations and rotations, following the energy gap law. Theoretical calculations reveal that strong stabilization of the S_1 state in eq-ax and eq-eq conformers is due to the planarization of the equatorial donor unit in the excited state (Fig. S6). Such CT state is further stabilized by the

dielectric response of the solvent; the calculated emission wavelength in toluene is 558 nm (2.22 eV) for eq-ax and 608 nm for eq-eq (2.04 eV) (Table S10 and S11). In a polar THF solvent, the CT emission are predicted at 656 nm (1.89 eV) and 720 nm (1.72 eV), respectively, but these states are most likely relaxing non-radiatively.

Tellurium-incorporated D–A–D compound **PTeZ-DBPHZ-PTeZ** shows fluorescence with a low quantum yield (Φ_{PL} 0.01–0.15) in diluted organic solvents, showing positive solvatochromic luminochromism (Fig. S4 and Table S4). In contrast to **PSeZ-DBPHZ-PSeZ**, the tellurium compound did not show dual emission in toluene, which is in good agreement with the domination of ax-ax conformer in this solvent (Fig. 3b) as suggested by the theoretical calculation (*vide infra*).

External Stimuli-Responsive Luminescence Properties

The photoluminescence behavior of **PSeZ-DBPHZ-PSeZ** under external stimuli was then investigated (Fig. 4). The as-prepared sample is a powdery crystalline sample, which shows sharp diffraction patterns in PXRD measurement (Fig. S9a). Upon the irradiation of UV light, the solid emits yellow PL (λ_{em} 576 nm, Φ_{PL} 0.04) (the inset photograph, Fig. 4a). Upon grinding the solid with a pestle and a mortar, the emission color drastically turned to deep-red, displaying a broad Gaussian emission spectrum (λ_{em} 671 nm, Φ_{PL} 0.09). (the inset photograph, Fig. 4a). The ground sample was found amorphous from the PXRD analysis (Fig. S9a). At a glance, this mechanochromic
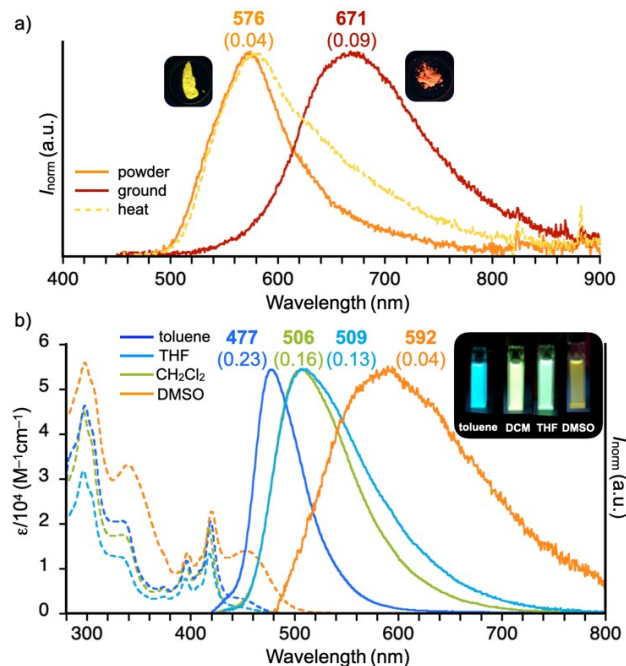

Fig. 4 a) Steady-state PL spectra of powder solids (as prepared), ground, and heated samples; b) Steady-state UV-vis absorption and PL spectra of solutions (c = 10⁻⁵ M, λ_{ex} = 400 nm) of **PSeOZ-DBPHZ-PSeOZ** prepared from various solvents. The inset photographs indicate the solutions taken under the irradiation of a UV light (λ = 365 nm).

ARTICLE

luminescence (MCL) behavior is very similar to that of its sulfur analogue.[26a] However, the response against thermal and vapor treatment of the ground Se-compound was found quite different from its sulfur atom (Fig. 4a). Upon heating the red-emitting ground sample on a hot plate at 200 °C for 15 min, the emission color reverted back to yellow, which was clearly seen on the PL spectra (Fig. 4a). The PXRD patterns of the heated sample were found almost superimposed with those of the as-prepared powder sample (Fig. S9a), confirming the recovery of the initial state. The fuming of the ground sample with organic vapor such as AcOEt and CHCl$_3$ also caused the similar recovery of yellow emission (Fig. S10). The PXRD analysis supported the recovery of the initial state (Fig. S9a). The deep-red emitting amorphous state was reproduced by grinding the heated and fumed samples. In contrast, the amorphous state of the sulfur analogue **PTZ-DBPHZ-PTZ** shows a much smaller blue-shift for heating (621 cm^{-1}) and fuming (1920 cm^{-1}) than that for selenium-compound (2458 cm^{-1}), and the deep-red emitting (ground sample) state does not revert back to yellow-emitting state.[26a] Therefore, the Se replacement for S atoms allows for high reversibility of the two-emitting states. To obtain deeper insights on this unique phenomenon, we compared the PXRD patters of the yellow-emitting crystalline sample with those predicted from the single-crystals of **G**, **Y**, and **O** (Fig. S9b). The comparison suggested that the eq-ax conformer would be the conformer contained in the yellow-emitting powder solids. Differential scanning calorimetry (DSC) of each solid sample revealed that the only the ground orange-emitting sample shows exothermic peaks at around 159 and 198 °C (Fig. S11), suggesting the ground sample is meta-stable state. Therefore, we can conclude that the enhanced reversibility of the initial state would be associated with the thermodynamic stability of the eq-ax conformer over eq-eq conformer in the aggregate states. Although this thermodynamic conformational preference appears to be inconsistence with that in solutions (Fig. 3b), there could be many factors controlling the thermodynamic preference of conformers in the solid states such as packing forces and intermolecular interactions.

In addition to the reversible MCL behavior in response to various stimuli, the selenium compound shows response to chemical stimuli. For example, the photoluminescence (PL) of the as-prepared **PSeZ-DBPHZ-PSeZ** turns off upon the treatment of vapor of trifluoroacetic acid (TFA), while the yellow PL turns on by fuming the solid with basic triethylamine (TEA) vapor (Fig. S12a). This turn/on-off cycle is reversible and repeatable (Fig. S12b). The selenium compound also shows redox-responsive emission color change through the reversible manipulation of the oxidation state of the Se atoms (i.e., Ar$_2$Se $\rightleftarrows$ Ar$_2$Se=O) (Fig. 4b, for the details of the redox procedures, see the ESI). It is worth mentioning that such Se-oxidation caused drastic change in absorption spectra, where the vibronic absorptions ascribed to the acceptor unit (ca. λ_{abs} 390 and 420 nm) are manifested and the CT absorption at around 450 nm is decreased (Fig. 4b) when compared to those of **PSeZ-DBPHZ-PSeZ** (Fig. 3c). The photoluminescence of the oxidized form (**PSeOZ-DBPHZ-PSeOZ**) displays more CT character showing larger positive solvatochromic shift (Fig. 4b) than that of Se(II) species (Fig. 3c), although the electronic donating ability of the phenoselenazine unit should be decreased. A possible rationale for explaining these contradicting spectra change would that the effect of the Se-oxidation caused drastic change in conformational preference from ax-ax to eq-based conformers, where the D and A units are almost completely decoupled, and thereby the charge-separated excited states are stabilized by the perpendicular D–A–D scaffold. This senario was supported by the conformational population by the theoretical calculation (eq-eq: 48%, eq-ax: 38%, ax-ax: 14%, see the Table S8).

In contrast to the behavior of the selenium compound, **PTeZ-DBPHZ-PTeZ** did not show photoluminescence in the solid state, probably due to the rapid ISC and IC accelerated by larger SOC in the condensed state, which could be caused by intermolecular heavy atom effect. Although the D–A–D tellurium compound does not show PL in the aggregated solid states, the compound exhibits blue-greenish PL in matrices with a long lifetime, indicating the room-temperature phosphorescence (RTP) (for the details, see the Time-Resolved Spectroscopy Section). More interestingly, the phenotellurazine donor (**PTeZ**) shows yellow (λ_{em} 556 nm, Φ_{PL} 0.09) and orange (λ_{em} 591 nm, Φ_{PL} 0.19) photoluminescence (PL) in the solid states (Fig. S13a) and Zeonex® matrix (Fig. S13b), respectively. The unexpected orange emission in the matrix was characterized with a long lifetime (τ_{avr} 11.7 μs under vacuum, Fig. S13c), which becomes shorter under the effect of air (τ_{avr} 5.7 μs, Fig. S13c). Given this emission peak almost matches with that of phosphorescence spectra acquired at 77 K (Fig. S13b), the orange emission from **PTeZ** should be RTP. Although the details of the origin of this unique RTP awaits further analysis, the large SOC, which was supported by the theoretical calculation (<S$_0$|H$_{SOC}$|T$_1$> 13.51 cm^{-1}, Table S14), should accelerate the irradiation from the T$_1$ to the S$_0$ state. It should be noted that **PTeZ** represents a new entry to organotellurium RTP family.[37]

Time-Resolved Spectroscopic Analysis

Initial steady-state photoluminescence analysis revealed the possibility of room-temperature phosphorescence (RTP) of both D–A–D compounds. Nevertheless, the full time-resolved analysis was indispensable to fully proof the photophysical mechanism. For that purpose, we investigated the photophysical properties of the solid-state layers of **PSeZ-DBPHZ-PSeZ** and **PTeZ-DBPHZ-PTeZ** in both a non-polar polymeric host Zeonex® and small molecular host CBP [4,4'-bis(N-carbazolyl)-1,1'-biphenyl] (Fig. 5). As supporting work, the analysis of pure donors (**PSeZ** and **PTeZ**) in Zeonex® matrix was also investigated (Fig. S14). The layers were deposited on sapphire substrate and analyzed in broad range of temperatures from 10 K up to 300 K. The short-lived emission of **PSeZ-DBPHZ-PSeZ** in Zeonex® matrix observed at 5.1 ns could be associated with emission from S$_1$ (^{1}LE) state and is similar at low (80 K, black line in Fig. 5a) and room-temperature (300 K, blue line in Fig. 5a). At further time delay,
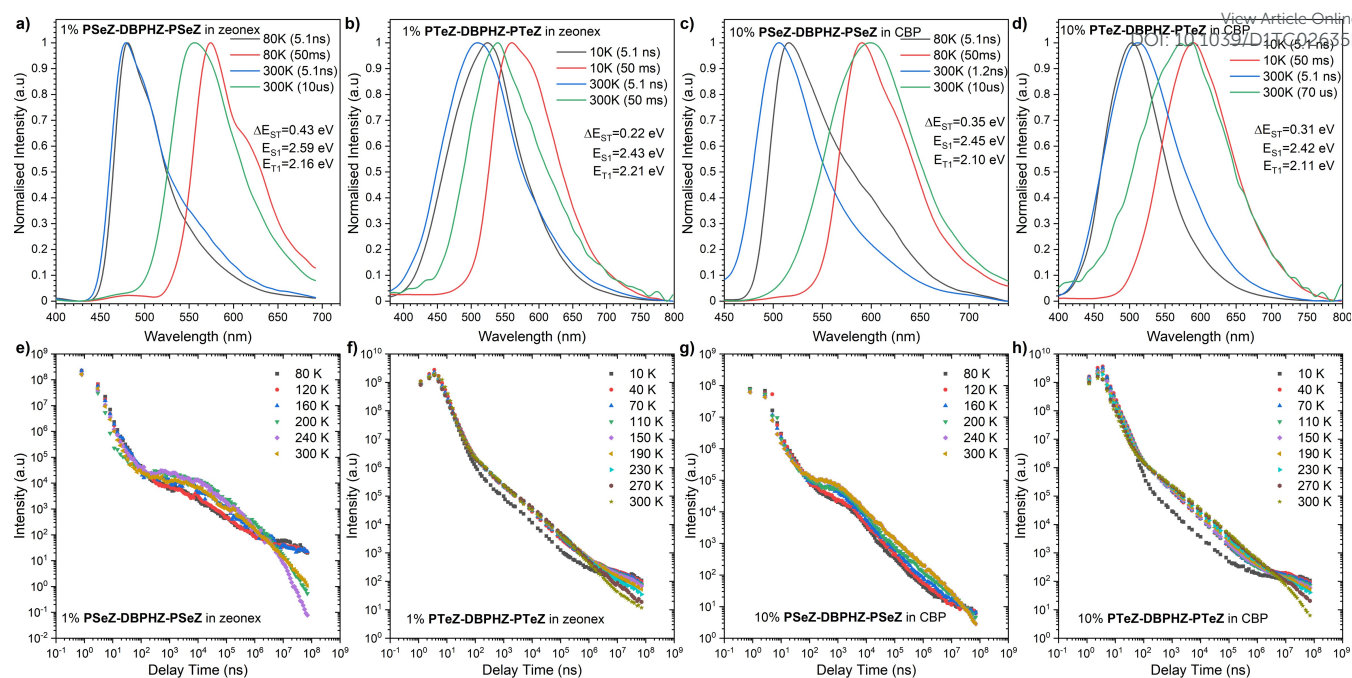
Fig. 5 Time-resolved spectroscopic analysis of **PSeZ-DBPHZ-PSeZ** and **PTeZ-DBPHZ-PTeZ** in matrices: Photoluminescence spectra of a) **PSeZ-DBPHZ-PSeZ** and b) **PTeZ-DBPHZ-PTeZ** in Zeonex®; c) **PSeZ-DBPHZ-PSeZ** and d) **PTeZ-DBPHZ-PTeZ** in CBP; Photoluminescence dacay of e) **PSeZ-DBPHZ-PSeZ** and f) **PTeZ-DBPHZ-PTeZ** in Zeonex®; g) **PSeZ-DBPHZ-PSeZ** and h) **PTeZ-DBPHZ-PTeZ** in CBP.

the emission is shifted to lower energies, and the phosphorescence is observed at low temperature (red line in Fig. 5a). As the temperature rises, the delayed emission is hypsochromically shifted, and the spectrum becomes broader (green and purple lines in Fig. 5a). Based on theoretical calculation, the ΔE_{ST} gap of **PSeZ-DBPHZ-PSeZ** in an ax-ax form is larger (490 meV) than the gap between T_1 and T_2 states (ΔE_{T1-T2} = 400 meV) (Fig. 7). Given these energy alignments and the SOC between the S_0–T_2 states (1.56 cm^{-1}), the temperature activated process (Fig. 5a and e) could be related with the processes comprising of ISC (from S_1 to T_1) followed by thermal reverse internal conversion (from T_1 to T_2) and the photo-irradiation from the T_1 and/or T_2 states.[29] Given the **PSeZ-DBPHZ-PSeZ** is admixture of ax-ax and eq-ax conforms (Fig. 3b), the energy transfer from the triplet excited state of ax-ax conformer to eq-ax conformer follwed by TADF emission from the ^{1}CT state possibly also occur.

Slightly different and complex behavior was observed for the **PTeZ-DBPHZ-PTeZ** in Zeonex® (Fig. 5b). The emissions at short delay times (in the ns region) are related with the emission from the S_1 (black and blue lines in Fig. 5b). As for the long-delayed emission (phosphorescence), the emission slightly shifted to the higher energy regime with the rise of temperature (red and green lines in Fig. 5b). Interestingly, while the energy level and the spectrum shape of the phosphorescence from T_1 of **PSeZ-DBPHZ-PSeZ** are similar to those of previously studied DBPHZ-cored D–A–D compounds,[24-29] the phosphorescence of **PTeZ-DBPHZ-PTeZ** appears to be much more similar to the phosphorescence of donor (**PTeZ**) (Fig. S14b). But, the calculation suggests that

similarity is coincidental. The T_1 state of the dominant ax-ax conformer of **PTeZ-DBPHZ-PTeZ** is localized on the acceptor (^{3}LE$_A$), and the donor retains its bent structure (Fig. 7f), while the T_1 state of **PTeZ** has a planarized geometry which stabilizes the excited state (Fig. S7). In the ax-ax conformer of the D-A-D compound, such planarization is not possible, due to the steric repulsion between D and A units. As the results, the energies of both triplet emissions of D and D–A–D compounds appear to be very close to each other.

More difficult processes to evaluate are involved in the photophysical properties of the investigated compounds inside CBP host, which was used for the fabrication and evaluation of OLED devices (Fig. 5c, d, g, and h). The emissions of both D–A–D compounds at shortest times are similar to those in Zeonex® matrix and should be ascribed to the localized excited singlet state (^{1}LE) in both low (80 K, black lines in Fig. 5c and d) and room temperature (300 K, blue lines in Fig. 5c and d). With both compounds, at low temperatures and long delay times, the phosphorescence is observed in the lower energy region than those in for Zeonex® layers, but the intensity is not that significant, suggesting it could be the emission from the lowest CT state. On one hand, the thermally activated emission processes are on the same energy levels like the process from the lowest ^{3}LE state, but the spectra are broader like the emission related to charge transfer process (Fig. 5c, d, g, and h). Such complex behavior is not usually observed, but as mentioned before, we probably observe the emission from T_1 and a higher triplet state (T_2).[29] The change of the host more affects the CT excited state energies to the lower level than LE states, thereby in CBP host both D–A–D compounds display

almost the same energy level. Fitting lifetimes of the D–A–D compounds and the donors are shown in Fig. S15 for reference, although the development of theoretical models to explain complex dynamics of such weak TADF and RTP emitters is undergoing.

Electrochemical Properties

The electrochemical behavior of the donors and D–A–D compounds in dichloromethane was investigated with cyclic voltammetry (CV) (Fig. S16). The cyclic voltammogram of **PSeZ-DBPHZ-PSeZ** displayed a reversible oxidation and reduction curves at $^{ox}E_{onset}$ = +0.31 V and $^{red}E_{onset}$ = −1.71 V (*vs.* Fc/Fc$^+$ redox couple), respectively. This electrochemical behavior looks typical for DBPHZ-cored D–A–D compounds (Fig. S15a).[24–29] On the other hand, the tellurium compound **PTeZ-DBPHZ-PTeZ** showed irreversible electrochemical redox behavior (Fig. S16b), indicating the less electrochemical instability than the sulfur[26a] and selenium analogues. Such tendency in the electrochemical analysis was previously reported in thiophene, selenophene, and tellurophene analogues, where the decomposition of the tellurophene ring was observed during the oxidation process.[38] When compared to the donors (**PSeZ** and **PTeZ**), distinct positive shift in the oxidation potential for the both D–A–D compounds by >0.3 V was observed (Fig. S16). The ionization potential (IP) and electron affinity (EA) for the **PSeZ-DBPHZ-PSeZ** and **PTeZ-DBPHZ-PTeZ** estimated from the CV experiment were estimated to be 5.41/3.39 eV and 5.38/3.35 eV, respectively.[39] When compared to the IP/EA of the sulfur analogue **PTZ-DBPHZ-PTZ** (5.33/3.38 eV)[26a] and oxygen analogue **POZ-DBPHZ-POZ** (5.36/3.38 eV),[25] the Se/Te replacement effect for S atoms in the D–A–D scaffold on electrochemical redox characters is very small. This can be explained by the kinetic process: the conformer with the lowest oxidation/reduction potential (eq-eq) is faster electrochemically oxidized/reduced on the electrode than other conformers (eq-ax and ax-ax) with higher oxidation/reduction potentials. What is also interesting, both D–A–D compounds undergo oxidative electropolymerization process after the third oxidation peak (Fig. S17a and b). It is also noted that only **PTeZ** donor forms polymer on the electrode (Fig. S17c).

OLED Fabrication and Characterization

To investigate the feasibility of fabricating OLED devices with the developed emitters, the thermal stability of the emitters was checked. The themogravimetry analysis (TGA) revealed their high thermal stability [**PSeZ-DBPHZ-PSeZ**: T_g (5 wt%) 383 °C under N$_2$ gas; **PTeZ-DBPHZ-PTeZ**: T_g (5 wt%) 412 °C under N$_2$ gas] (Fig. S18 and S19). This indicates the feasibility of thermal sublimation process of OLED devices under vacuum. The investigated compounds were used as dopant in the CBP matrix. The following two OLED structures were deposited using high-vacuum thermal evaporators, Dev1: ITO/NPB (40 nm)/10% **PSeZ-DBPHZ-PSeZ** in CBP (25 nm)/TPBi (50 nm)/LiF (1 nm)/Al (100 nm); Dev2: ITO/NPB (40 nm)/10% **PTeZ-DBPHZ-PTeZ** in CBP (25 nm)/TPBi (50 nm)/LiF (1 nm)/Al (100 nm). The
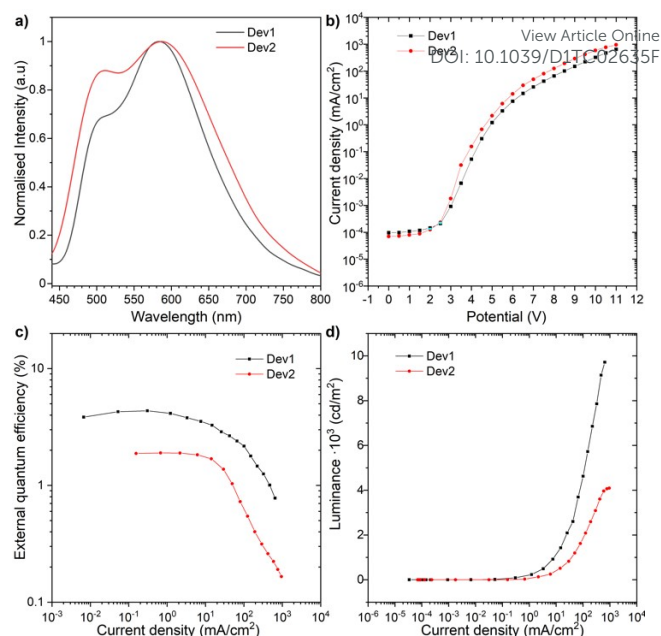

Fig. 6 The characteristics of the OLED devices: a) Electroluminescence spectra; b) Current density-bias characteristics; c) EQE-current density characteristics; d) Luminance-current density characteristics.

performances and photophysical results of the fabricated OLED devices were investigated and compared in order to evaluate emissive pathways that boost the efficiency properties. Most importantly, dual-emissive property of the emitters was manifested in both OLED devices (Fig 6a). Such behavior is not usual, but taking into the time-resolved spectroscopic analysis data (Fig. 5), the higher-energy emission at around λ_{em} 500 nm in both cases would be related with the electroluminescence from the S$_1$ (^{1}LE) state and the lower-energy emission at around λ_{em} 600 nm with the RTP from the ^{3}LE state. In other words, fluorescence and room-temperature phosphorescence (RTP) processes are involved in the electroluminescence.[40] In both cases, the RTP contribution in overall emission, which was estimated from the comparing the area of emission spectra acquired in aerated and degassed conditions, is higher than 90%, and therefore the mostly related factor for the efficiency of the device should be the phosphorescence process. The highest external quantum efficiency (EQE) of the OLEDs was obtained with **PSeZ-DBPHZ-PSeZ** (4.35%), where the device with tellurium derivative **PTeZ-DBPHZ-PTeZ** showed a lower EQE of 1.89% (Fig. 6c). These EQE values may not be that high, when compared with the OLED devices with existing heavy-atom-containing RTP organic emitters. But, if we assume that the overall PLQY for those compounds is less than 10%, it would suggest we obtained as highest efficiency as possible. On the other hand, the devices exhibit quite high luminance as for selenium and tellurium derivatives with up to 10,000 cd/m^2 for **PSeZ-DBPHZ-PSeZ** and more than 4,000 cd/m^2 for **PTeZ- DBPHZ-PTeZ**-based device.

Journal Name

ARTICLE

Theoretical Calculations

To obtain deeper insights into the developed emitters, theoretical calculations were performed at the density functional theory level for the **PSeZ-DBPHZ-PSeZ** and **PTeZ-DBPHZ-PTeZ** compounds (see the ESI for details). Ground state geometry optimizations of the different conformers associated with a weighting procedure using Boltzmann factors at 300 K allowed us to conclude that all the three **PSeZ-DBPHZ-PSeZ** conformers (i.e., ax-ax, ax-eq, and eq-eq) should coexist at room temperature, with the ax-ax conformation being the most stable (55% probability),

followed by eq-ax (38%) and eq-eq (7%) (Table S5). In contrast, only two **PTeZ-DBPHZ-PTeZ** conformers are expected to be present at room temperature, namely ax-ax (98%) and eq-ax (2%) (Table S6). As such, we noticed that one of the effects of heavy atom substitution from S to Se and Te is a progressive dominance of ax-ax conformations (Fig. 3b), due to the deepening of the potential energy surface in this particular geometry. Importantly, conformational preference is not significantly affected by solvents, as shown in Table S7.

Excited state calculations in toluene revealed that for all **PSeZ-DBPHZ-PSeZ** conformers the T_1 states correspond to a localized excitation (^3LE_A) state of the acceptor unit. On the other hand, S_1 states correspond to charge transfer (CT) states in all but the ax-ax conformer, as evidenced by the natural transition orbitals (NTOs) presented in Fig. 7a, b, and c.
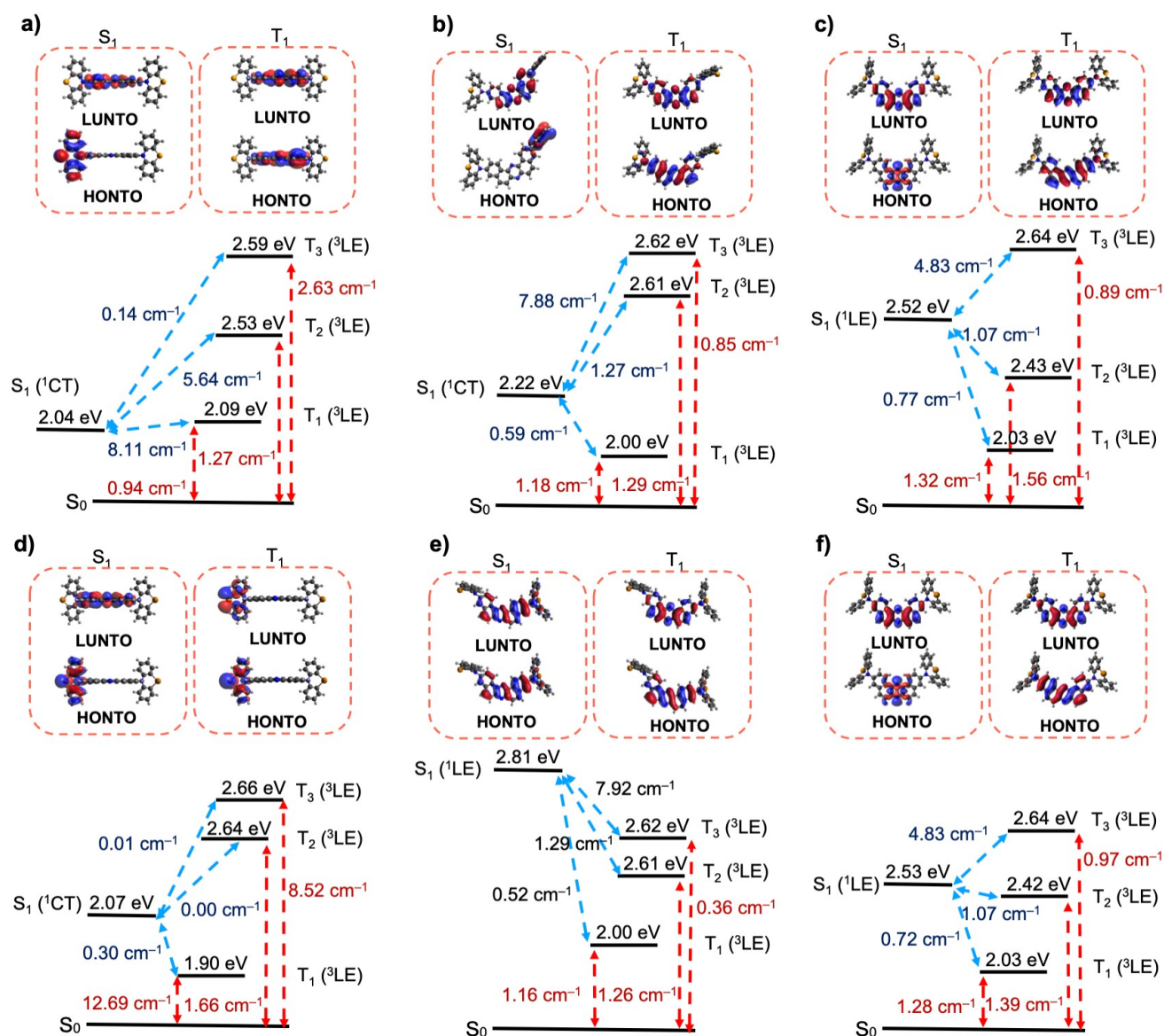

Fig. 7 Natural transition orbitals (NTOs) for the S_1 and T_1 states along with corresponding energy levels for the three conformations of a) eq-eq, b) eq-ax, and c) ax-ax conformers of **PSeZ-DBPHZ-PSeZ** in toluene; d) eq-eq, e) ax-eq, and f) ax-ax conformers of **PTeZ-DBPHZ-PTeZ** in toluene; Blue and red arrows correspond to the spin-orbit couplings (SOCs) between S_1–T_n and T_n–S_0, respectively.

ARTICLE

However, Fig. 7d, e, and f show that for eq-ax and ax-ax **PTeZ-DBPHZ-PTeZ** conformers, both S_1 and T_1 states correspond to localized excitations in the acceptor portion of the molecule, whereas the eq-eq conformer presents an S_1 state with CT character and a T_1 state that is localized in the donor unit. In particular, this difference is reflected in the significantly higher oscillator strength associated with S_0-S_1 transitions of the **PTeZ-DBPHZ-PTeZ** molecule. In fact, the S_0-S_1 transitions for both the eq-eq and eq-ax conformations of **PSeZ-DBPHZ-PSeZ** are predicted to be forbidden (zero oscillator strength). These characteristics, in addition to the aforementioned population of the different conformers, account for the observed differences in the absorption spectrum of the S, Se and Te-containing D–A–D compounds.

Calculated emission energies from the S_1 state in the ax-ax conformers of both compounds predict fluorescence at around 2.5 eV (Table S12), in agreement with experimental results (Fig. 3c and Fig. S4b). A lower energy band in **PSeZ-DBPHZ-PSeZ** fluorescence spectrum is also predicted at 2.2 eV to result from CT emission from the eq-ax conformer (Table S12). Such second band is not observed for **PTeZ-DBPHZ-PTeZ**, however (Table S12). This behavior stems from the fact that the donor unit of the eq-ax Se compound undergoes planarization in the S_1 state (Fig. S6), resulting in a lower energy CT state that is further strongly stabilized by a polarizable environment.[41] Such planarization is not seen in the Te compounds, for which the S_1 emission energy in the eq-ax conformer is much larger (2.81 eV, Fig. 7e).

Phosphorescence energies calculated for both D–A–D compounds are also very similar and predicted to lie around 2.0 eV (Table S13). This is due to the fact that T_1 states in the ax-ax conformation of both molecules correspond to localized excitations in the acceptor unit (Fig. 7c and f). For the pure **PSeZ** and **PTeZ** donor fragments, phosphorescence energies are predicted at 2.3 eV and 1.9 eV, respectively (Table S14). As such, the experimentally observed similarity in phosphorescence energies between the Te-containing D–A–D compound and the **PTeZ** fragment does not necessarily imply that phosphorescence in **PTeZ-DBPHZ-PTeZ** stems from the donor unit.

Spin-orbit coupling calculations have also been performed for all molecules in toluene using the T_1 geometry (Fig. 7; The NOTs for T_2 and T_3 are shown in Fig. S8). These calculations revealed that S_0-T_1 spin-orbit couplings are affected mostly by substitution of the Se atoms for Te rather than by conformation. This can be seen from the overall larger couplings calculated for **PTeZ-DBPHZ-PTeZ** conformers when compared to **PSeZ-DBPHZ-PSeZ**. For the ax-ax conformation, which is the most likely to be present, S_1-T_1 couplings are found to be around 0.7 cm^{-1} for both molecules. The S_1-T_1 transition in this conformer is allowed, partially due to the fact that it corresponds to a transition between two different LE states (n-π^* and π-π^*).

Conclusions

In conclusion, we have developed a new family of photofunctional dibenzo[*a,j*]phenazine-cored twisted donor-acceptor–donor (D–A–D) compounds having Se and Te bridging atoms in the electronic donors. Of the developed compounds, selenium-containing D–A–D compound **PSeZ-DBPHZ-PSeZ** displays unique multi-photofunctionality of polymorph-dependent multi-photoluminescence, single molecular white emission, various external-stimuli-responsive luminochromism, and unusual dual emission of fluorescence and room-temperature phosphorescence in thin films and OLED devices. In contrast, the tellurium analogue **PTeZ-DBPHZ-PTeZ** are non-emissive in the solid states, probably due to the accelerated ISC and the following IC. Despite the quenching in the condensed phase, the tellurium compound shows RTP in host matrices and OLED devices. Also, unexpectedly we have found out that the donor **PTeZ** represents a new family of RTP-displaying organotellurium compounds. From the careful comparison of the organoselenium/tellurium compounds with the lighter chalcogen analogues, the most striking effect of replacing with Se and Te for S in the DBPHZ-cored D–A–D twisted scaffold involves the drastic increase in the preference of ax-oriented conformers over the eq ones, due to transannular electronic interaction. This conformational change strongly affects the absorption and photoluminescence profiles in solutions, the reversibility in external-stimuli-induced phase transition, and excited states energy parameters such as ΔE_{ST}, ΔE_{TT}, and spin-orbit coupling (SOCs) that govern the fate of the mechanisms involved in the excited states. The knowledge obtained through this research would pave the new avenue for multi-photofunctional organoselenium and organotellurium materials.

Acknowledgements

Notes and references

1 (*a*) C. W. Nogueira, G, Zeni and J. B. T. Rocha, *Chem. Rev.*, 2004, **104**, 6255–6285; (*b*) B. Banerjee and M. Koketsu, *Coor. Chem. Rev.*, 2017, **339**, 102–127; (*c*) *Organoselenium Compounds in Biology and Medicine: Synthesis, Biological and Therapeutic Treatments*, ed. V. K. Jain and K. I. Priyadarsini, The Royal Society of Chemistry, Croydon, UK, 2018; (*d*) T. Wirth, *Angew. Chem., Int. Ed.*, 2015, **54**, 10074–10076.

2 (*a*) M. R. Detty, A. E. Friedman and A. R. A. Oseroff, *J. Org. Chem.*, 1994, **59**, 8245–8250; (*b*) Z. Chen, H. Lai, L. Hou and T. Chen, *Chem. Commun.*, 2020, **56**, 179–196.

3 (*a*) S. T. Manjare, Y. Kim and D. G. Churchill, *Acc. Chem. Res.*, 2014, **47**, 2985–2998; (*b*) S. Panda, A. Panda and S. S. Zade, *Coord. Chem. Rev.*, 2015, **300**, 86–100.

4 (*a*) L. Engman, *Acc. Chem. Res.*, 1985, **18**, 274–279; (*b*) *The Chemistry of Organic Selenium and Tellurium Compounds*, ed. Z. Rappoport, Wiley-VCH, Weinheim, 2012, vol. 3.

5 (*a*) M. R. Detty, F. Zhou and A. E. Friedman, *J. Am. Chem. Soc.*, 1996, **118**, 313–318; (*b*) M. Oba, Y. Okada, K. Nishiyama and W. Ando, *Org. Lett.*, 2009, **11**, 1879–1881; (*c*) E. A. Alberto, L. M. Muller and M. R. Detty, *Organometallics*, 2014, **33**, 5571–5581; (*d*) Y. Okada, M. Oba, A. Arai, K. Tanaka, K. Nishiyama and W. Ando, *Inorg. Chem.*, 2010, **49**, 383–385; (*e*) M. Godoi, M. W. Paixão and A. L. Braga, *Dalton Trans.*, 2011, **40**, 11347–11355; (*f*) V. Rathore, C. Jose and S. Kumar, *New. J. Chem.*, **2019**, *43*, 8852–8864.

6 (*a*) J. Xia, T. Li, C. Lu and H. Xu, *Macromolecules*, 2018, **51**, 7435–7455; (*b*) S. Yamago, *Bull. Chem. Soc. Jpn.*, 2020, **93**, 287–298.

7 (*a*) L. V. Romashov and V. P. Ananikov, *Chem. Eur. J.*, 2013, **19**, 17640–17660; (*b*) L. Wang, W. Cao and H. Xu, *ChemNanoMat*, 2016, **2**, 479–488; (*c*) W. Cao and H. Xu, *Mater. Chem. Front.*, 2019, **3**, 2010–2017.

8 (a) K. Selvakumar and H. B. Singh, *Chem. Sci.*, 2018, **9**, 7027–7042; (*b*) M. Fourmigué and A. Dhaka, *Coord. Chem. Rev.*, 2020, **403**, 213084/1–17; (*c*) N. Biot and D. Bonifazi, *Coord. Chem. Rev.*, 2020, **413**, 213243/1–22.

9 (*a*) T. Otsubo and K. Takimiya, in *Handbook of Thiophene-Based Materials: Applications in Organic Electronics and Photonics*; ed. I. F. Perpepichka and D. F. Perepichka, John Wiley & Sons Ltd, Chichester, UK, 2009, pp321–340; (*b*) L. Zhang, S. M. Fakhouri, F. Liu, J. C. Timmons, N. A. Ran and A. L. Briseno, *J. Mater. Chem.*, 2011, **21**, 1329–1337; (*c*) T. Okamoto, M. Mitani, C. P. Yu, C. Mitsui, H. Yamagishi, H. Ishii, G. Watanabe, S. Kumagai, D. Hashizume, S. Tanaka, M. Yano, T. Kushida, H. Sato, K. Sugimoto, T. Kato and J. Takeya, *J. Am. Chem. Soc.*, 2020, **142**, 14974–14984.

10 (*a*) J. G. Manion, J. R. Panchuk and D. S. Seferos, *Chem. Rec.*, 2019, **19**, 1113–1122; (*b*) M. Jeffries-EL, B. M. Kobilka and B. J. Hale, *Macromolecules*, 2014, **47**, 7253–7271.

11 S. A. Gregory, A. K. Menon, S. Ye, D. S. Seferos, J. R. Reynolds and S. K. Yee, *Adv. Energy Mater.*, 2018, **8**, 1802419/1–8.

12 C. C. Hoover and D. S. Seferos, *Chem. Sci.*, 2019, **10**, 9182–9188.

13 K. Wittel and R. Manne, *Theoret. Chim. Acta (Berl.)*, 1974, **33**, 347–349.

14 M. A. El-Sayde, *Acc. Chem. Res.*, 1968, **1**, 8–16.

15 R. D. Pensack, Y. Song, T. M. McCormick, A. A. Jahnke, J. Hollinger, D. S. Seferos and G. D. Scholes, *J. Phys. Chem. B*, 2014, **118**, 2589–2597.

16 D. de Sa Pereira, D. R. Lee, N. A. Kukhta, K. H. Lee, C. L. Kim, A. S. Batsanov, J. Y. Lee and A. P. Monkman, *J. Mater. Chem. C*, 2019, **7**, 10481–10490.

17 B. H. Drummond, G. C. Hoover, A. J. Gillett, N. Aizawa, W. K. Myers, B. T. McAllister, S. T. E. Jones, Y.-J. Pu, D. Credgington and D. S. Seferos, *J. Phys. Chem. C*, 2020, **124**, 6364–6370.

18 D. R. Lee, K. H. Lee, W. Shao, C. L. Kim, J. Kim and J. Y. Lee, *Chem. Mater.*, 2020, **32**, 2583–2592.

19 (*a*) Y. Tao, K. Yuan, T. Chen, P. Xu, H. Li, R. Chen, C. Zheng, L. Zhang and W. Huang, *Adv. Mater.*, 2014, **26**, 7931–7958; (*b*) F. B. Dias, T. J. Penfold and A. P. Monkman, *Methods Appl. Fluoresc.*, 2017, **5**, 012001; (*c*) Z. Yang, Z. Mao, Z. Xie, Y. Zhang, S. Liu, J. Zhao, J. Xu, Z. Chi and M. P. Aldred, *Chem. Soc. Rev.*, 2017, **46**, 915–1016; (*d*) M. Y. Wong, E. Zysman-Colman, *Adv. Mater.*, 2017, **29**, 1605444; (*e*) M. Sarma and K.-T. Wong, *ACS Appl. Mater. Interfaces*, 2018, **10**, 19279–19304; (*f*) X. K. Chen, D. Kim and J.-L. Brédas, *Acc. Chem. Res.*, 2018, **51**, 2215–2224; (*g*) Y. Liu, C. Li, Z. Ren, X. Yan, M. R. Bryce, *Nat. Rev. Mater.*, 2018, **3**, 18020.

20 (*a*) S. Mukherjee and P. Thilagar, *Chem. Commun.*, 2015, **51**, 10988–11003; (*b*) M. Baroncini, G. Bergamini and P. Ceroni, *Chem. Commun.*, 2017, **53**, 2081–2093; (*c*) P. Ceroni, *Chem.*, 2016, **1**, 524–526; (*d*) A. Forni, E. Lucenti, C. Botta and E. Cariati, *J. Mater. Chem. C*, 2018, **6**, 4603–4626; (*e*) H. Yuasa and S. Kuno, *Bull. Chem. Soc. Jpn.*, 2018, **91**, 223–229; (*f*) G. Zhan, Z. Liu, Z. Bian and C. Huang, *Front. Chem.*, 2019, **7**, 305/1–6. (*g*) H. Ma, A. Lv, S. Wang, Z. An, H. Shi and W. Huang, *Ann. Phys.* (Berlin), 2019, **531**, 1800482/1–14.

21 H. Chen, Y. Deng, X. Zhu, L. Wang, L. Lv, X. Wu, Z. Li, Q. Shi, A. Peng, Q. Peng, Z. Shuai, Z. Zhao, H. Chen and H. Huang, *Chem. Mater.*, 2020, **32**, 4038–4044.

22 L. Xu, K. Zhou, H. Ma, A. Lv, D. Pei, G. Li, Y. Zhang, Z. An, A. Li and G. He, *ACS Appl. Mater. Interfaces*, 2020, **12**, 18385–18394.

23 (*a*) Y. Sagara, and T. Kato, *Nat. Chem.*, 2009, **1**, 605–610; (*b*) A. Pucci, R. Bizzarri, G. Ruggeri, *Soft Matter*, 2011, **7**, 3689–3700; (*c*) Z. Chi, X. Zhang, B. Xu, X. Zhou, C. Ma, Y. Zhang, S. Liu and J. Xu, *Chem. Soc. Rev.*, 2012, **41**, 3878–3896. (*d*) Z. Ma, Z. Wang, M. Geng, Z. Xu and X. Jia, *ChemPhysChem*, 2015, **16**, 1811–1828; (*e*) Y. Sagara, S. Yamane, M. Mitani, C. Weder and T. Kato, *Adv. Mater.*, 2016, **28**, 1073–1095; (*f*) S. Xue, X. Qiu, Q. Sun, W. Yang, *J. Mater. Chem. C*, 2016, **4**, 1568–1578; (*g*) P. Xue, J. Ding, P. Wang and R. Lu, *J. Mater. Chem. C*, 2016, **4**, 6688–6706; (*h*) C. Wang and Z. Li, *Mater. Chem. Front.*, 2017, **1**, 2174–2194.

24 (*a*) P. Data and Y. Takeda, *Chem. Asian J.*, 2019, **14**, 1613–1636; (*b*) Y. Takeda, P. Data and S. Minakata, *Chem. Commun.*, 2020, **56**, 8884–8894.

25 P. Data, P. Pander, M. Okazaki, Y. Takeda, S. Minakata, and A. P. Monkman, *Angew. Chem.*, *Int. Ed.*, 2016, **55**, 5739–5744.

26 (*a*) M. Okazaki, Y. Takeda, P. Data, P. Pander, H. Higginbotham, A. P. Monkman and S. Minakata, *Chem. Sci.*, 2017, **8**, 2677–2686; (*b*) P. Data, M. Okazaki, S. Minakata and Y. Takeda, *J. Mater. Chem. C*, 2019, **7**, 6616–6621; (*c*) Y. Takeda, H. Mizuno, Y. Okada, M. Okazaki, S. Minakata, T. Penfold and G. Fukuhara, *ChemPhotoChem*, 2019, **3**, 1203–1211.

27 Y. Takeda, T. Kaihara, M. Okazaki, H. Higginbotham, P. Data, N. Tohnai and S. Minakata, *Chem. Commun.*, 2018, **54**, 6847–6850.

28 H. Yamagishi, S. Nakajima, J. Yoo, M. Okazaki, Y. Takeda, S. Minakata, K. Albrecht, K. Yamamoto, I. Badía-Domínguez, M. M. Oliva, M. C. R. Delgado, Y. Ikemoto, H. Sato, K. Imoto, K. Nakagawa, H. Tokoro, S.-i. Ohkoshi and Y. Yamamoto, *Commun. Chem.*, 2020, **3**, 118/1–8.

29 H. F. Higginbotham, M. Okazaki, P. de Silva, S. Minakata, Y. Takeda and P. Data, *ACS Appl. Mater. Interfaces*, 2021, **13**, 2899–2907.

Journal of Materials Chemistry C Accepted Manuscript

ARTICLE

Journal Name

30   (*a*) S. Izumi, H. F. Higginbotham, A. Nyga, P. Stachelek, N. Tohani, P. de Silva, P. Data, Y. Takeda and S. Minakata, *J. Am. Chem. Soc.*, 2020, **142**, 1482–1491; (*b*) A. Nyga, S. Izumi, H. F. Higginbotham, P. Stachelek, S. Pluczyk, P. de Silva, S. Minakata, Y. Takeda and P. Data, *Asian J. Org. Chem.*, 2020, **9**, 2153–2161; (c) S. Izumi, A. Nyga, P. de Silva, N. Tohnai, S. Minakata, P. Data and Y. Takeda, *Chem. Asian J.*, 2020, **15**, 4098–4103.

31   Y. Takeda, M. Okazaki and S. Minakata, *Chem. Commun.*, 2014, **50**, 10291–10294.

32   T. Junk and K. J. Irgolic, *Heterocycles*, 1989, **28**, 1007–1013.

33   C. Cremer, M. Goswami, C. K. Rank, B. de Bruin and F. W. Patureau, *Angew. Chem.*, *Int. Ed.*, 2021, **60**, 6451–6456.

34   H. Naito, Y. Morisaki and Y. Chujo, *Angew. Chem.*, *Int. Ed.*, 2015, **54**, 5084–5087.

35   G. te Velde, F. M. Bickelhaupt, E. J. Baerends, C. F. Guerra, S. J. A. van Gisbergen, J. G. Snijders and T. Ziegler, *J. Compt. Chem.*, 2001, **22**, 931–967.

36   Z. Chen, C.-L. Ho, L. Wang, W. Y. Wong, *Adv. Mater.,* 2020, **32**, 1903269/1–45.

37   (*a*) G. He, W. T. Delgado, D. J. Schatz, C. Merten, A. Mohammadpour, L. Mayr, M. J. Ferguson, R. McDonald, A. Brown, K. Shankar, E. Rivard, *Angew. Chem.*, *Int. Ed.*, 2014, **53**, 4587–4591; (*b*) A. Kremer, C. Aurisicchio, F. de Leo, B. Ventura, J. Wouters, N. Armaroli, A. Barbieri and D. Bonifazi, *Chem. Eur. J.*, 2015, **21**, 15377–15387; (*c*) L. Xu, G. Li, T. Xu, W. Zhang, S. Zhang, S. Yin, Z. An and G. He, *Chem. Commun.*, 2018, **54**, 9226–9229; (*d*) M. Jiang, J. Guo, B. Liu, Q. Tan, B. Xu, *Org. Lett.*, 2019, **21**, 8328–8333.

38   M. Lapkowski, R. Motyka, J. Suwiński and P. Data, P. *Macromol. Chem. Phys.*, 2012, **213**, 29–35.

39   IP = (5.1 + $^{ox}E_{onset}$/V) [eV]; EA = (5.1 + $^{red}E_{onset}$/V) [eV]. (*a*) C. M. Cardona, W. Li, A. E. Kaifer, D. Stockdale and G. Bazan, *Adv. Mater*., 2011, **23**, 2367–2371; (*b*) J.-L. Bredas, *Mater. Horiz.*, 2014, **1**, 17–19.

40   M. Shimizu and T. Sakurai, *ChemPlusChem*, 2020, **86**, 446–459.

41   P. de Silva, *J. Phys. Chem. Lett.*, 2019, **10**, 5674–5679.

Journal of Materials Chemistry C Accepted Manuscript

Please do not adjust margins